

Review

MgB₂ thin films by hybrid physical–chemical vapor deposition

X.X. Xi^{a,b,*}, A.V. Pogrebnyakov^{a,b}, S.Y. Xu^a, K. Chen^a, Y. Cui^a, E.C. Maertz^a,
C.G. Zhuang^{a,b,c}, Qi Li^a, D.R. Lamborn^d, J.M. Redwing^{b,d}, Z.K. Liu^b,
A. Soukiassian^b, D.G. Schlom^b, X.J. Weng^b, E.C. Dickey^b, Y.B. Chen^e, W. Tian^e,
X.Q. Pan^e, S.A. Cybart^f, R.C. Dynes^f

^a Department of Physics, The Pennsylvania State University, University Park, PA 16802, USA

^b Department of Materials Science and Engineering, The Pennsylvania State University, University Park, PA 16802, USA

^c Department of Physics, Peking University, Beijing 100871, PR China

^d Department of Chemical Engineering, The Pennsylvania State University, University Park, PA 16802, USA

^e Department of Materials Science and Engineering, The University of Michigan, Ann Arbor, MI 48109, USA

^f Department of Physics, University of California, Berkeley, CA 94720, USA

Received 15 December 2006; received in revised form 29 January 2007; accepted 29 January 2007

Available online 14 February 2007

Abstract

Hybrid physical–chemical vapor deposition (HPCVD) has been the most effective technique for depositing MgB₂ thin films. It generates high magnesium vapor pressures and provides a clean environment for the growth of high purity MgB₂ films. The epitaxial pure MgB₂ films grown by HPCVD show higher-than-bulk T_c due to tensile strain in the films. The HPCVD films are the cleanest MgB₂ materials reported, allowing basic research, such as on magnetoresistance, that reveals the two-band nature of MgB₂. The carbon-alloyed HPCVD films demonstrate record-high H_{c2} values promising for high magnetic field applications. The HPCVD films and multilayers have enabled the fabrication of high quality MgB₂ Josephson junctions.

© 2007 Elsevier B.V. All rights reserved.

PACS: 74.70.Ad; 81.15.–z; 74.78.–w

Keywords: Magnesium diboride; Film growth; Epitaxy; Transition temperature; Upper critical field; Josephson junctions

Contents

1. Introduction	23
2. Key requirements in deposition of MgB ₂ films	23
3. Hybrid physical–chemical vapor deposition	24
4. Clean epitaxial HPCVD films	25
4.1. Structural properties	25
4.2. High T_c , low resistivity, and high critical current	25
4.3. Strain-induced E_{2g} phonon softening	26
4.4. Large anisotropic magnetoresistance	27

* Corresponding author. Address: Department of Physics, The Pennsylvania State University, University Park, PA 16802, USA. Tel.: +1 814 863 5350; fax: +1 814 865 3604.

E-mail address: xxx4@psu.edu (X.X. Xi).

4.5. Low microwave surface resistance	28
4.6. Absence of dendritic magnetic instability	29
4.7. Studies of controlled disorders	30
5. Carbon-alloyed HPCVD films	30
5.1. Deposition process and microstructures	30
5.2. Superconducting properties	30
6. Polycrystalline MgB ₂ films	31
7. Epitaxial boride heterostructures	33
8. Josephson junctions and SQUIDS	33
9. Concluding remarks	34
Acknowledgements	35
References	35

1. Introduction

Magnesium diboride, MgB₂, is an exciting superconductor [1]. It is a conventional BCS superconductor, in which the Cooper pairs are formed through electron–phonon coupling [2], with a high transition temperature T_c of 39 K [1]. It has multiple bands with weak interband scattering: the two-dimensional σ bands and the three-dimensional π bands [3]. They couple to the B–B stretch modes of E_{2g} symmetry with different strengths, resulting in different superconducting energy gaps [4,5]. The existence of the “two bands” and “two gaps” not only effects various properties of MgB₂ [6,7], it also leads to new physics that does not exist in single-band superconductors [8–13]. For electronic applications, the high T_c of MgB₂ allows operation of MgB₂ devices and circuits above 20 K, substantially reducing the cryogenic requirements compared to the Nb-based superconducting electronics, which have to operate at 4.2 K [14,15]. MgB₂ Josephson junctions [16] and superconducting quantum interference devices (SQUIDS) [17] with excellent properties well over 20 K have been demonstrated. For applications in high magnetic field, carbon-alloyed MgB₂ films have shown higher upper critical field H_{c2} values than those of the Nb-based superconductors at all temperatures [18]. MgB₂ is of particular interest for magnets in cryogen-free magnetic resonance imaging (MRI) systems [19]. It is further recognized that the high T_c and low resistivity make MgB₂ an attractive material for RF cavity applications [20,21].

High quality MgB₂ thin films are important for both fundamental research and electronic, high-field, and RF cavity applications. Much effort has been devoted to the deposition of MgB₂ thin films and tremendous progress has been achieved by various deposition techniques [22]. The deposition techniques used for MgB₂ films include high-temperature *ex situ* annealing of B or Mg–B precursor films in Mg vapor [23–29], intermediate-temperature *in situ* annealing of Mg–B precursor films [30–36], low-temperature *in situ* deposition [36–40], and high- and intermediate-temperature *in situ* deposition [41–43]. An analysis of the pros and cons of each techniques has been given in

Ref. [22]. Of all these techniques, hybrid physical–chemical vapor deposition (HPCVD) [43,44] has been the most effective one for MgB₂ films. The HPCVD MgB₂ films on single crystal substrates such as *c*-cut SiC and sapphire are epitaxial [43,45]. The pure films show T_c values at almost 42 K, higher than the bulk samples [46], and residual resistivity much lower than 1 $\mu\Omega$ cm [9]. When alloyed with carbon, the upper critical field H_{c2} of the HPCVD films increases dramatically from that of the pure films to reach over 60 T at low temperatures [18,47]. Similar results have been obtained in polycrystalline MgB₂ films on polycrystalline substrates [48,49], including metallic substrates. A wide range of works by various groups using HPCVD films have played important roles in the research of MgB₂.

In this paper, we describe the principles and key elements of the HPCVD technique and discuss the properties of MgB₂ films deposited using HPCVD, including clean epitaxial films, carbon-alloyed films, polycrystalline films, and multilayers of MgB₂ with other materials. A short summary of MgB₂ Josephson junctions using HPCVD films will be presented, while additional information can be found in the review on epitaxial MgB₂ tunnel junctions and SQUIDS by Brinkman and Rowell [50].

2. Key requirements in deposition of MgB₂ films

The most important requirement for the deposition of MgB₂ films is to provide a sufficiently high Mg vapor pressure for the thermodynamic phase stability of MgB₂ at elevated temperatures. Fig. 1 is a Mg pressure–temperature phase diagram calculated by Liu et al. [51]. The MgB₂ film deposition parameters should fall within the growth window marked by “Gas + MgB₂” where the thermodynamically stable phases are MgB₂ and Mg gas. The Mg pressures for this growth window are very high for temperatures necessary for *in situ* epitaxial growth of MgB₂ films. For example, deposition at 750 °C requires a Mg pressure greater than 44 mTorr to keep MgB₂ thermodynamically stable. To satisfy the thermodynamic phase stability requirement, the high-temperature *ex situ* annealing approach heats the B or Mg–B precursor film with Mg

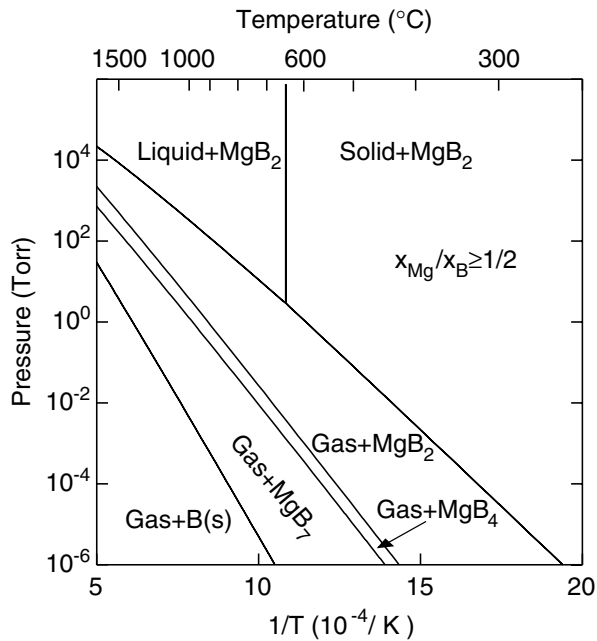


Fig. 1. The pressure–temperature phase diagram for the Mg:B atomic ratio $x_{\text{Mg}}/x_{\text{B}} \geq 1/2$. The region marked by “Gas + MgB₂” represent the growth window for MgB₂ films (from Ref. [51]).

bulk in an enclosure [23]; the intermediate-temperature *in situ* annealing technique relies on the local Mg vapor pressure generated by the heating of excess Mg [30]; and the low-temperature *in situ* deposition approach avoids the requirement of high Mg vapor pressure by going to low temperatures [37]. The most critical step in the success of the HPCVD technique is its capability of generating high Mg vapor pressure at around 700 °C [43].

It should be noted that the pressure–temperature phase diagram is identical for all Mg/B ratios $x_{\text{Mg}}/x_{\text{B}} \geq 1:2$ [51]. MgB₂ is a line compound and as long as the Mg/B ratio is above the stoichiometric 1:2, extra Mg will be in the gas phase and be evacuated. Also, once MgB₂ is formed, Fan et al. showed that a significant kinetic barrier needs to be overcome for MgB₂ to thermally decompose [52], which is much more difficult than predicted by the thermodynamics. This is very convenient in practice, as one does not have to be overly concerned about maintaining a high Mg pressure during the cooling stage of the MgB₂ film deposition.

Clean environment for growth and pure sources of Mg and B are other key requirements for the growth of high quality MgB₂ films. MgB₂ is highly susceptible to contaminations with oxygen and carbon. For example, *in situ* deposition of MgB₂ at 250–300 °C results in insulating films if the background pressure is equal or worse than 3×10^{-8} Torr due to the reaction of Mg with oxygen [39]. Carbon is a common contaminant, mostly from the source materials such as in sputter or laser ablation targets. Carbon impurity reduces T_c of MgB₂ [53] and prevents the deposition of clean MgB₂ films. Being able to meet the requirements of clean environment and pure sources is another critical step in the success of the HPCVD technique.

3. Hybrid physical–chemical vapor deposition

Fig. 2a is a schematic of the HPCVD setup [44]. It consists of a water cooled quartz tube reactor and a susceptor, which is inductively heated. During the deposition, the carrier gas is purified H₂ with a flow rate of the order of 400 sccm to 1 slm at a pressure of about 100 Torr. The high total pressure makes it possible to generate a high Mg vapor pressure necessary for the phase stability of MgB₂. The reducing environment is important for preventing oxidation during the deposition. Bulk pure Mg is used as the Mg source. As shown in the figure, several pieces of bulk Mg are placed next to the substrate on the top of the susceptor. When the susceptor is heated to 550–760 °C, which is high enough for epitaxial growth of MgB₂, pure Mg pieces are also heated, which generates a high Mg vapor pressure in the vicinity of the substrate. Diborane, B₂H₆, is used as the high purity boron source. MgB₂ film starts to grow when the boron precursor gas, 1000 ppm – 5% B₂H₆ in H₂, is introduced into the reactor. The flow rate of B₂H₆/H₂ mixture ranges from 5 to 250 sccm, which controls the growth rate of the MgB₂ film, ranging from several Å/s to over 50 Å/s. The film growth stops when the boron precursor gas is switched off. Since the technique combines physical vapor deposition (heated bulk Mg as the Mg source) with chemical vapor deposition (B₂H₆ as the boron source), it was named hybrid physical–chemical vapor deposition.

Computational simulations of the boron film growth in the HPCVD reactor were carried out by Lamborn et al. [54]. The transport model assumed laminar flow in the reactor tube and the buoyancy driven convection currents was also considered. The physical properties of the gases were calculated using the ideal gas law and the kinetic theory of gases. The properties of the solid materials used in the reactor were also inputs in the simulation. The simulation result for the velocity magnitude profile in the reactor is

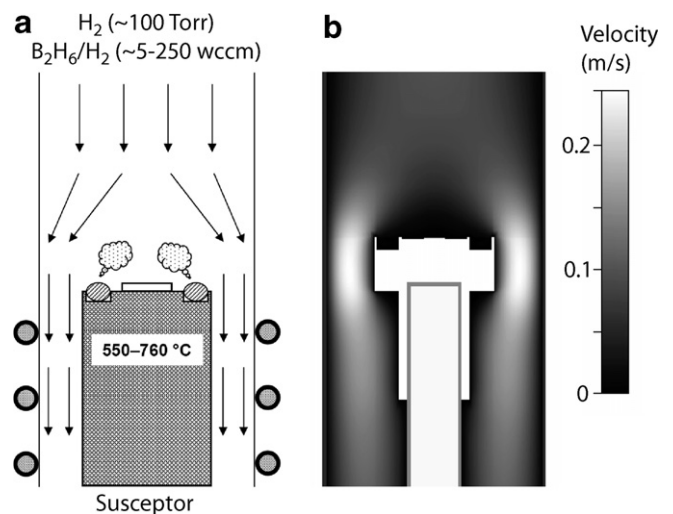


Fig. 2. (a) Schematic of the HPCVD system. (b) Calculated gas velocity profile in the reactor near the susceptor (from Ref. [54]).

shown in Fig. 2b for typical operating conditions used for MgB_2 growth. It shows that a stagnant layer above the face of the susceptor develops as the flow field changes from an unobstructed pipe to annular flow and the free stream velocity increases between the susceptor and reactor wall.

The addition of heated Mg pieces will make the simulation much more complicated, but the result of Fig. 2b can offer some hints to the environment near the substrate during the MgB_2 deposition. Because the Mg pieces and the substrate are located where the stagnant gas flow region is in Fig. 2b, it is likely that a slow gas flow keeps a significant amount of the Mg vapor released from the bulk Mg in this region, giving rise to a high Mg vapor pressure around the substrate. Further modeling studies are currently underway to investigate these effects. The precise value of the Mg vapor pressure during the MgB_2 deposition is not easily known. However, as long as it is above the minimum pressure necessary for the MgB_2 phase stability and as long as the Mg:B ratio is larger than 1:2, the automatic composition control in an adsorption-controlled growth, as is the case for MgB_2 , keeps the composition of the film stoichiometric [51].

4. Clean epitaxial HPCVD films

4.1. Structural properties

The high deposition temperatures in HPCVD made possible by the high Mg vapor pressure result in excellent epitaxy and crystallinity in the MgB_2 films deposited by this technique [43,45]. Fig. 3 shows a high-resolution transmission electron microscope (HRTEM) image for the interface between a MgB_2 film and (0001) 6H-SiC substrate. The insets are selected area electron diffraction (SAED) patterns from the film (top) and substrate (bottom). The result

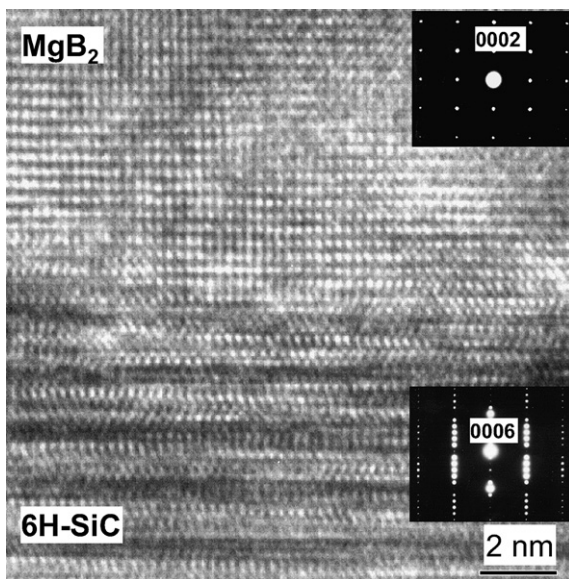


Fig. 3. A high-resolution TEM image of the film/substrate interface in a MgB_2 film on (0001) 6H-SiC substrate. Top inset: SAED pattern from the film. Bottom inset: SAED pattern from the substrate.

shows that the MgB_2 film grows epitaxially on the SiC substrate with an orientation relationship of $(000\bar{1}) [1120]\text{MgB}_2 \parallel (0001)[11\bar{2}0]\text{SiC}$. The interface is atomically sharp and there is no obvious reaction at the interface. High quality epitaxial growth has also been confirmed by X-ray diffraction measurements, where both the out-of-plane alignment, shown by the $\theta-2\theta$ scans, and the in-plane alignment, shown by the ϕ scans, with the substrate lattice were observed [43,45]. The rocking curves for both $\theta-2\theta$ and ϕ scans are sharp, indicating good crystallinity.

MgB_2 has a hexagonal structure with $a = 3.086 \text{ \AA}$ and $c = 3.524 \text{ \AA}$ [1]. The (0001) oriented SiC (for the 4H polytype $a = 3.073 \text{ \AA}$ and for the 6H polytype $a = 3.081 \text{ \AA}$) offers a close lattice match for the epitaxial growth of c -axis oriented MgB_2 films [45]. The c -cut sapphire ($a = 4.765 \text{ \AA}$) is another suitable substrate for epitaxial films, however the lattice mismatch is larger and the hexagonal MgB_2 lattice is rotated by 30° to match that of the substrate [43]. Occasionally, the 30° in-plane rotation also exists in some grains in MgB_2 films on (0001) SiC substrate. In MgB_2 films on sapphire, oxide layers have been observed at the film/substrate interface [43,55,56], while the interface between MgB_2 film and SiC substrate is often free from oxides [57].

For MgB_2 tunnel junctions, it is desirable to tunnel from ab -plane to ab -plane, thus from σ band to σ band, to take advantage of the large σ gap [58]. While it is a challenge to grow ab oriented films, we have found that MgB_2 films grow with tilted c -axis on some substrates with surfaces of rectangular lattice. For example, tilted c -axis epitaxial MgB_2 films have been shown on (110) YSZ [59] and (211) MgO substrate [60].

4.2. High T_c , low resistivity, and high critical current

The highly reducing H_2 ambient and the high purity Mg and B sources used in HPCVD lead to very clean MgB_2 thin films [61]. Fig. 4 shows a resistivity vs temperature

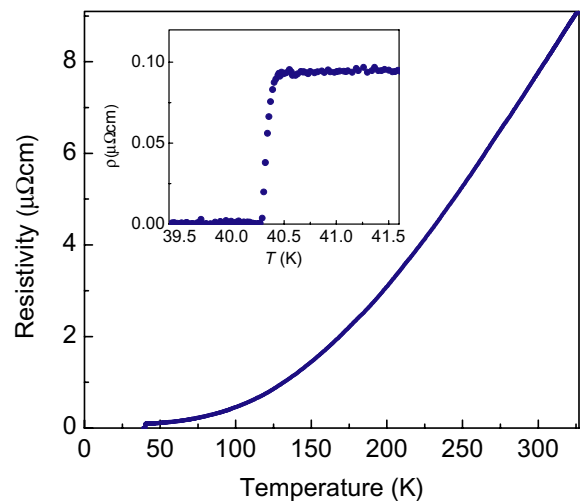


Fig. 4. Resistivity vs temperature curve for a 7700 \AA MgB_2 thin film on sapphire substrate. The inset shows details near the superconducting transition.

curve for a 7700 Å MgB₂ thin film on sapphire substrate. It shows a T_c over 40 K, and a low residual resistivity ρ_0 of less than 0.1 $\mu\Omega$ cm, leading to a residual resistivity ratio RRR of over 80. Fig. 5 shows residual resistivity vs film thickness for a series of MgB₂ films. A linear dependence on 1/thickness is observed, indicating that the mean free path in this series of MgB₂ films is mainly limited by the scattering at the film surface and the film/substrate interface. The pure HPCVD films are cleaner than the reported single crystals [62] and bulk samples [63]. By fitting the normal-state magnetoresistance data [64], it was found that

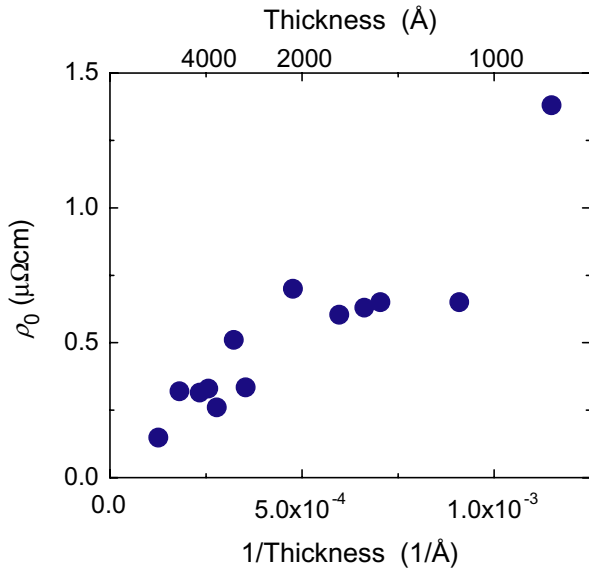


Fig. 5. Residual resistivity as a function of film thickness for a series of MgB₂ films.

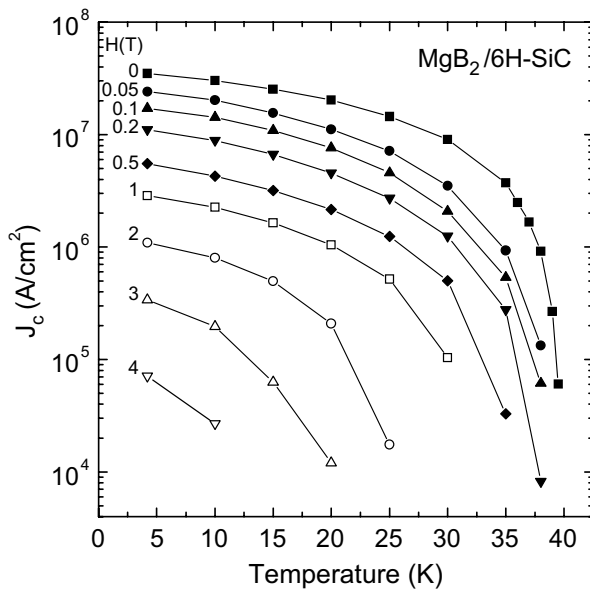


Fig. 6. Transport J_c vs temperature for a MgB₂ film on SiC substrate measured under different applied magnetic fields (from Ref. [45]).

both the σ and π bands of pure HPCVD films are in the clean limit [65].

The critical current density J_c of the pure HPCVD films is high. Fig. 6 shows the result of a transport J_c measurement of a patterned bridge of 20 μm width in a MgB₂ film on SiC substrate. The self-field J_c is 3.4×10^7 A/cm² at 4.2 K [45], not very far from the depairing critical current density in MgB₂ [66]. However, J_c is suppressed quickly by the applied magnetic field indicating a lack of pinning, a consequence of the cleanness and excellent crystallinity of the films.

4.3. Strain-induced E_{2g} phonon softening

Fig. 4 clearly shows a T_c higher than that in the bulk MgB₂ [1]. This is due to the strain-induced E_{2g} phonon softening that enhances the electron–phonon interaction [46]. We have found that on both sapphire and SiC substrates, T_c increases with increasing film thickness [61]. In Fig. 7, zero-resistance T_c is plotted as a function of a and c lattice parameters for a series of MgB₂ films on sapphire (squares) and SiC (circles) substrates. On each substrates, larger a lattice parameters correspond to thicker films, and T_c increases with increasing a lattice parameters even

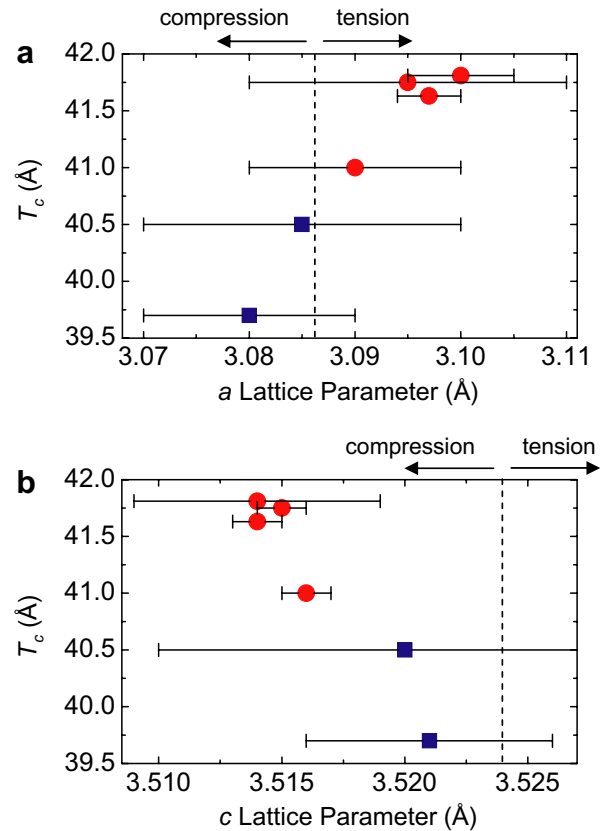


Fig. 7. Dependence of zero-resistance T_c on (a) a lattice parameter and (b) c lattice parameter. The square symbols are from films on sapphire, and the circles are from films on SiC substrate. On each substrate, the a lattice parameter increases with film thickness.

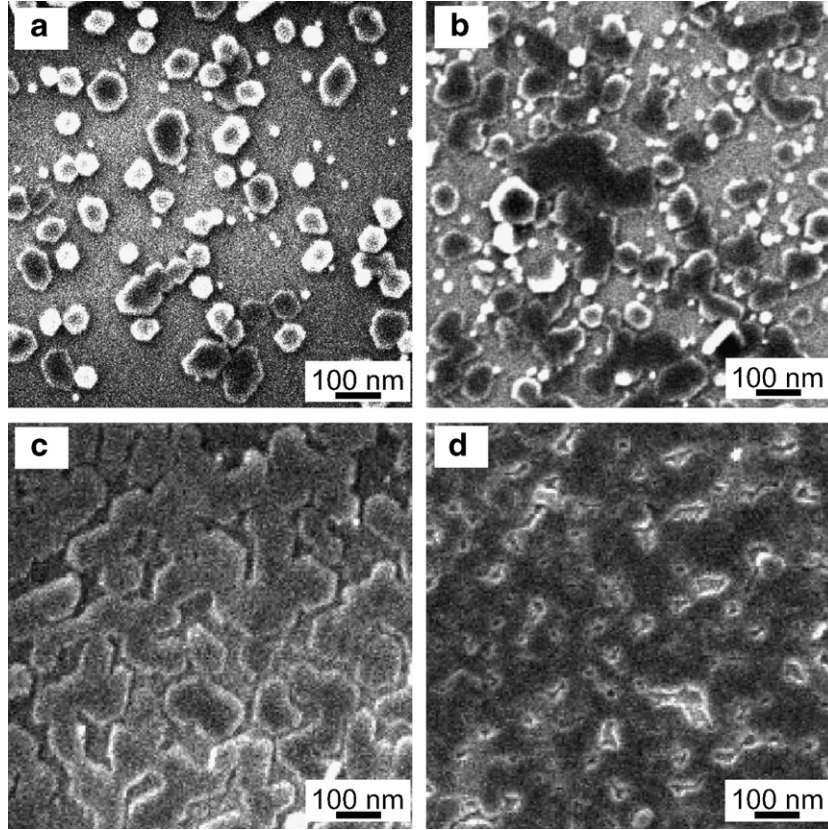


Fig. 8. SEM images of four MgB_2 films with nominal thicknesses of (a) 65 Å, (b) 70 Å, (c) 150 Å, and (d) 200 Å on SiC substrate.

thought the data are from films on different substrates. It is evident that T_c of the MgB_2 films increases with in-plane tensile strain. The highest zero-resistance T_c obtained in the HPCVD films is 41.8 K on SiC substrate, well above the bulk value.

The growth mode of the HPCVD MgB_2 films is the Volmer–Weber mode [46], i.e. the initially nucleated discrete islands coalesce when the films grow thicker. This is clearly demonstrated by the scanning electron microscope (SEM) images of four MgB_2 films of different thicknesses on SiC substrate shown in Fig. 8. At the beginning of the growth, islands of hexagonal shape form on the substrate, which grow and merge at larger film thickness. At 200 Å, the islands have largely coalesced and the substrate coverage is almost complete. Coalescence tensile strain occurs in metallic films grown in the Volmer–Weber mode, and the tensile strain increases with the film thickness [67,68].

First-principles calculations show that the tensile strain causes the bond-stretching E_{2g} phonon mode to soften. According to the McMillan–Allen–Dynes analysis, $T_c \propto \omega e^{-f(\lambda, \hat{\mu})}$, where ω is the phonon frequency, $f(\lambda, \hat{\mu}) = (1 + \lambda)/(\lambda - \hat{\mu})$, $\hat{\mu}$ is similar to the Coulomb repulsion μ^* , and λ is the electron–phonon coupling constant. If considering only the maximum element in the electron–phonon coupling matrix for MgB_2 , i.e. the electron–phonon coupling between two σ band electrons [5], $\lambda \propto 1/\omega^2$. The softening of the E_{2g} phonon mode (decrease in ω) leads to a

large increase in λ . Because λ is in the exponent in the T_c formula, this increase more than compensates the decrease in the prefactor ω , thus an overall increase in T_c is achieved [46]. Since the discovery of superconductivity in MgB_2 , many techniques have been used without success to further increase T_c . Despite the theoretical prediction that the T_c of 39 K is the maximum for MgB_2 [69], our result is an example where T_c of MgB_2 is increased from the bulk value by lowering the E_{2g} phonon frequency, which points to a possible avenue to achieve higher T_c in MgB_2 .

4.4. Large anisotropic magnetoresistance

Magnetoresistance is a powerful probe into the electronic structures of a solid [70–72]. In very clean epitaxial MgB_2 films grown by HPCVD, we have observed a large anisotropic normal-state magnetoresistance ($\Delta\rho/\rho_0 = 136\%$ for the $H\parallel ab$ direction at 18 T) [9]. This is a direct result of the multiband nature of MgB_2 and the cleanness of the HPCVD films. For a single-band free-electron system, the Hall field exactly balances the Lorentz force and therefore there is no magnetoresistance. However, if there are two or more bands of different carriers, the Hall field cannot exactly cancel the Lorentz force and there will be magnetoresistance [70–72]. As MgB_2 has four Fermi surfaces with both electrons and holes [3], large transverse magnetoresistance can be expected in MgB_2 . The low

resistivity of the films is critical. In samples with residual resistivity $>1\text{--}2\ \mu\Omega\ \text{cm}$, the maximum magnetoresistance is only a few percent.

In Fig. 9, the angular dependence of magnetoresistance of a MgB_2 film is shown for different magnetic fields at $T = 45\ \text{K}$. It has a complex behavior with a minimum at $H\parallel ab$. This anisotropy undergoes a crossover at around $100\ \text{K}$ to a high-temperature behavior where the magnetoresistance minimum is at $H\perp ab$ and the $H\parallel ab$ direction becomes a maximum. The magnetoresistance anisotropy reflects the Fermi surface topology and the relative scattering rates of the different bands. As the temperature increases, the electron–phonon coupling for the σ bands is stronger than the π bands, resulting in the change of the relative scattering rate between the bands. The strong contribution of the σ bands to magnetoresistance at low temperatures changes to the dominance of the π bands at high temperatures. Pallecchi et al. have solved the Boltzmann equation for MgB_2 using the relative ratio of the scattering rate in the σ and π bands as the key parameters, which explained the main features of the angular dependence of magnetoresistance shown here [64].

The multiband effect also causes the breakdown of the Kohler’s rule. According to the Kohler’s rule, if only one relaxation time τ exists in a solid, $\Delta\rho/\rho_0$ from different temperatures should collapse to a single curve in a Kohler plot, $\Delta\rho/\rho_0$ vs H/ρ_0 [72]. The experimental results did not show the conventional collapse [9]. This is the consequence of multiple bands with different relaxation times, which depend differently on temperature due to different electron–phonon coupling [73].

The result on normal-state magnetoresistance is an excellent demonstration of new physical phenomena in MgB_2 due to the multiband nature that do not exist in single-band superconductors [8]. Other examples include the possible collective excitation corresponding to small fluctuations of the relative phase of two condensates (the “Legg-

ett mode”) [12,13,74,75]; vortices with arbitrary fractional flux quantum [76]; breakdown of the applicability of the anisotropic Ginzburg–Landau theory [77]; and phase textures and voltage oscillations induced by current in non-equilibrium [10] or equilibrium conditions [11]. Clean single-crystalline epitaxial HPCVD films provide a clean medium for the studies of these phenomena.

4.5. Low microwave surface resistance

The microwave surface resistance R_s of HPCVD films has been measured by Jin et al. by a sapphire resonator technique at $18\ \text{GHz}$ [78]. Fig. 10 shows the dependence of R_s on ρ_0 at $15\ \text{K}$ (solid) and $20\ \text{K}$ (open) for MgB_2 films from different sources. Surface resistance decreases linearly with decreasing residual resistivity. The HPCVD films show the lowest ρ_0 , and consequently the lowest surface resistance. An R_s ($18\ \text{GHz}$) of $230\ \mu\Omega$ was obtained at $15\ \text{K}$. The clean HPCVD films also show the shortest penetration depth $\lambda(0)$ of lower than $50\ \text{nm}$.

From the measured temperature dependence of surface impedance Z_s , the superconducting gap $\Delta(0)$ was extracted. Fig. 11 is the dependence of $\Delta(0)$ on ρ_0 of different MgB_2 films. In microwave measurements of MgB_2 , only the π gap can be obtained [79]. The figure shows that the cleaner the films (corresponding to a smaller ρ_0), the smaller the $\Delta(0)$ is. This is the result of weak interband scattering. When the films become dirtier, the interband scattering becomes stronger. Putti et al. have shown that the enhanced interband scattering causes the σ gap to decrease and the π gap to increase [80]. The clean HPCVD films have the lowest π gap among the samples measured, indicating very weak interband scattering in these films. The small π -gap value, as well as the large σ -gap value, in HPCVD films have also been measured in MgB_2 -barrier–Pb Josephson junctions [60], again indicating weak interband scattering.

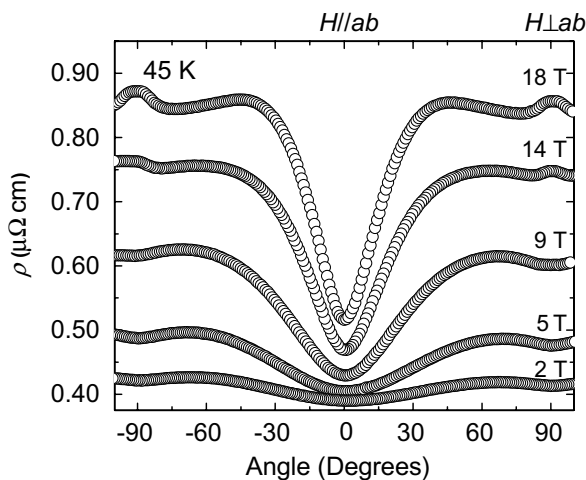


Fig. 9. Resistivity of a MgB_2 film as a function of the angle between the applied magnetic field and the film surface measured at $T = 45\ \text{K}$. The results are shown for different applied magnetic fields (from Ref. [9]).

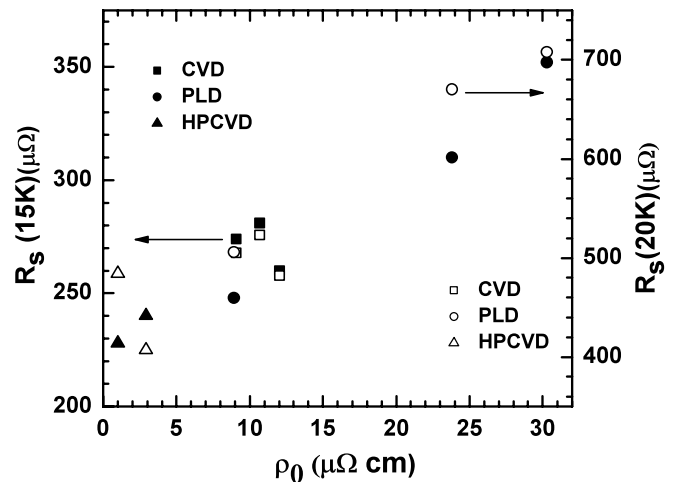


Fig. 10. Dependence of R_s on ρ_0 at $15\ \text{K}$ (solid) and $20\ \text{K}$ (open) for MgB_2 films from different sources (from Ref. [78]).

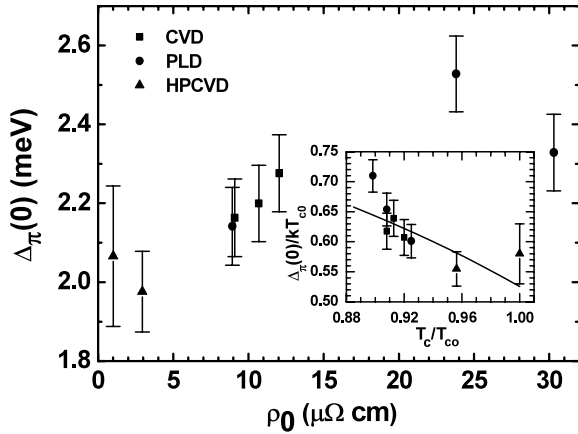


Fig. 11. Dependence of the π -band energy gap on ρ_0 for MgB_2 films from different sources (from Ref. [78]). The inset shows $\Delta_{\pi}(0)/T_{c0}$ as a function of T_c/T_{c0} , where T_{c0} is the T_c of an HPCVD film.

For applications of superconductors in microwave devices, low microwave nonlinearity is important for power handling capabilities [81]. Dahm and Scalapino have calculated the nonlinearity properties of MgB_2 , and found that the existence of the two bands leads to large nonlinearity, however it can be improved by manipulation of the interband and intraband scattering [82]. The nonlinear response of HPCVD MgB_2 films were measured by Cifariello et al. using a dielectrically loaded copper cavity operating at

7 GHz [83]. The result shows the intrinsic two-band s -wave behavior predicted by Dahm and Scalapino.

The surface resistance of superconductors increases quadratically with frequency, therefore the low R_s advantage of a superconductor over normal metal disappears at high frequencies [84]. For example, R_s of high-temperature superconductor YBCO at 77 K becomes higher than that of Cu above about 200 GHz [84]. In a time domain THz spectroscopy measurement, Jin et al. found that in HPCVD films, the surface resistance is still lower than Cu at frequencies around 1–2 THz [85]. This shows a great potential of MgB_2 for THz electronic applications.

4.6. Absence of dendritic magnetic instability

In many thin film and bulk MgB_2 samples strong flux instabilities at low temperatures have been reported [86,87]. Using magneto-optical imaging (MOI) techniques, Johansen et al. showed that below 10 K dendritic structures of magnetic flux form abruptly in pulsed-laser-deposited MgB_2 films when the magnetic field penetrates into the film [87]. This corresponds to flux jumps, an avalanche process where flux motion dissipates heat and leads to a local temperature rise which reduces local pinning and facilitates further flux motion [88]. Because of the dendritic flux jumps, the hysteresis loop of the magnetization is

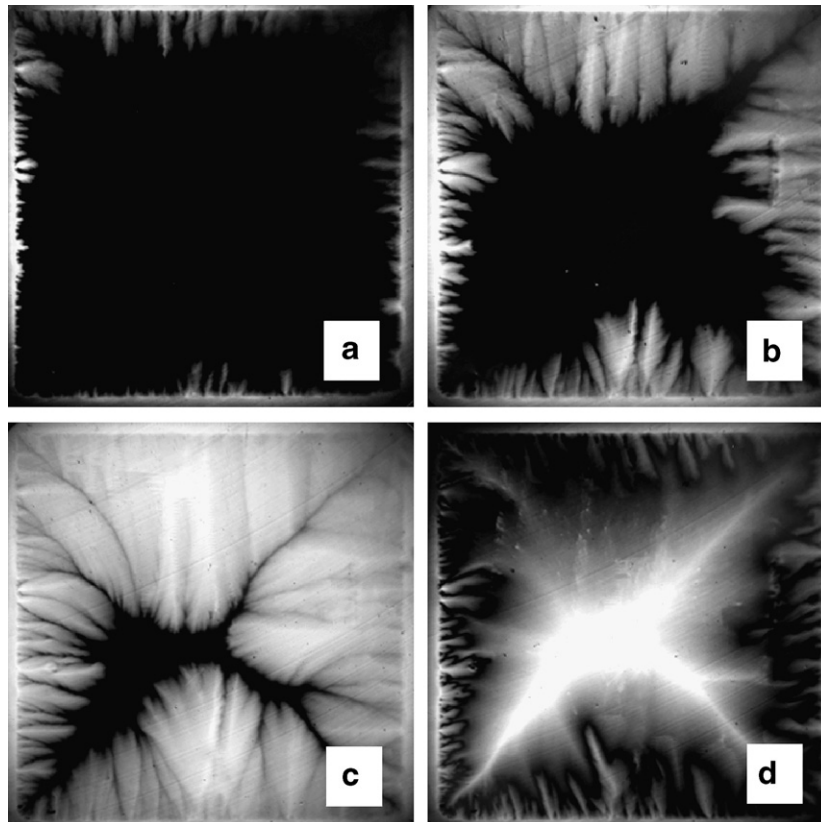


Fig. 12. Magneto-optical images of a zero-field-cooled pure HPCVD film at $T = 4.2$ K. The perpendicular applied field $B =$ (a) 10 mT, (b) 20 mT, (c) 40 mT, and (d) 0 (reduced from 0.1 T) (from Ref. [90]).

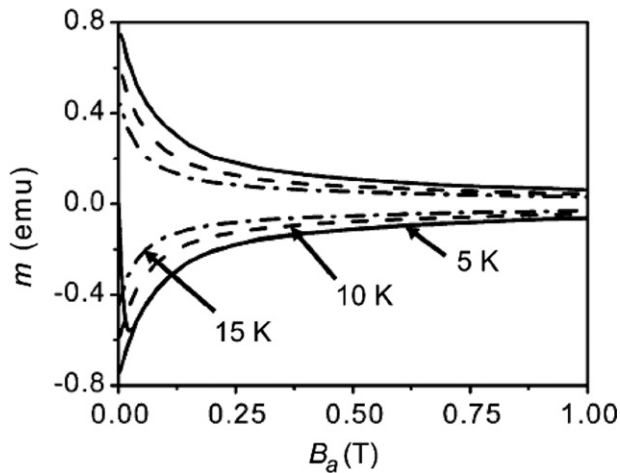


Fig. 13. Magnetization curves of the clean HPCVD film at $T = 5, 10,$ and 15 K (from Ref. [90]).

suppressed at low temperature and low field, indicating suppressed J_c .

In pure HPCVD MgB_2 films, however, the low temperature dendritic flux jumps are absent [89,90]. Fig. 12 are MOI images showing regular flux penetration and trapping patterns in a zero-field-cooled (ZFC) pure HPCVD film at 4.2 K. With increasing field, the magnetic flux penetrates gradually and uniformly into the sample from the edges, consistent with critical state models. When the field is decreased, the flux exits the sample in the same manner. Fig. 13 shows a part of the magnetization hysteresis loop for the pure HPCVD film at 5, 10, and 15 K. There is no suppressed J_c at 5 K and the width of the loops decreases as the temperature increases due to the lower J_c at higher temperatures. These results are in striking contrast to the earlier reports showing dendritic flux jumps [87] and suppressed hysteresis loop width [86] at low temperatures for MgB_2 . It is evident that the cleanness of the HPCVD film and its low normal state resistivity enhance the magnetic stability at low temperatures.

4.7. Studies of controlled disorders

The clean and highly crystalline HPCVD films provide excellent starting materials to introduce disorders in a controlled manner and study the effects of disorder on properties of MgB_2 . The ways to introduce disorder have included heavy ion (200 MeV Ag) irradiation [91], α -particle irradiation [92,93], and neutron irradiation [65]. These studies have contributed to both fundamental understanding of the two-band effect in MgB_2 and the technologically important issue of increasing H_{c2} and flux pinning.

5. Carbon-alloyed HPCVD films

Although clean MgB_2 films are desirable for many fundamental studies and applications, good superconducting properties in high magnetic field require the superconduc-

tors to be dirty. Clean MgB_2 has low H_{c2} [7], but in high resistivity MgB_2 films H_{c2} is substantially higher [94]. Because of the multiple impurity scattering channels and the two-gap nature of superconductivity in MgB_2 , H_{c2} can be enhanced well above the estimate $H_{c2}(0) = 0.69T_c H'_{c2}(T_c)$ of one-gap theory. The HPCVD technique can not only produce very clean pure MgB_2 films, it is also an effective way to dope or alloy the films for better properties in magnetic field. In this section, we summarize the deposition and properties of carbon-alloyed MgB_2 films by HPCVD.

5.1. Deposition process and microstructures

The carbon-alloyed MgB_2 films are produced in the same apparatus shown in Fig. 2 and using the same procedure described above except that a metalorganic magnesium precursor, bis(methylcyclopentadienyl)magnesium ((MeCp)₂Mg), is added to the carrier gas [95]. A secondary hydrogen flow is passed through a (MeCp)₂Mg bubbler, and the amount of carbon in the film is controlled by the flow rate of the secondary hydrogen gas flow. A correlation between the nominal carbon concentration in the film and the secondary hydrogen flow rate was established by measuring a series of carbon-alloyed MgB_2 films with wavelength dispersive X-ray spectroscopy.

Cross-sectional TEM shows that the carbon-alloyed MgB_2 films have a granular structure [95]. They consist of columnar nano-grains of $\text{Mg}(\text{B}_{1-x}\text{C}_x)_2$ with a preferential c -axis orientation. The in-plane alignment with the substrate remains, but it is much disordered, and foreign phases exist between the grains. Although a definitive identification of the foreign phases at the grain boundaries is difficult, they are most likely B_4C , B_8C , or B_{13}C_2 [96]. Only a small portion of carbon in the film is doped into the MgB_2 grain and most of them is contained in the grain boundaries.

X-ray diffraction shows that in the carbon-alloyed MgB_2 films both c and a axes expand with increasing carbon concentration (see Fig. 14 [95]). This is qualitatively different from those in carbon-doped single crystals and filaments, where the a -axis lattice constant decreases but that of c -axis remains almost constant for all the carbon concentrations [97,98]. This structural characteristic may be critical for the much higher H_{c2} values in carbon-alloyed HPCVD films than in the bulk samples discussed below [47].

5.2. Superconducting properties

When the MgB_2 films are alloyed with carbon, their resistivity increases dramatically and T_c is gradually suppressed with increasing carbon concentration [95]. The T_c decrease is accompanied by the hardening of the E_{2g} phonon mode [99]. The suppression of T_c is much slower and the increase of resistivity much faster in the carbon-alloyed HPCVD films than in carbon-doped single crystals [97] and filaments [98], indicating again that only a small portion of

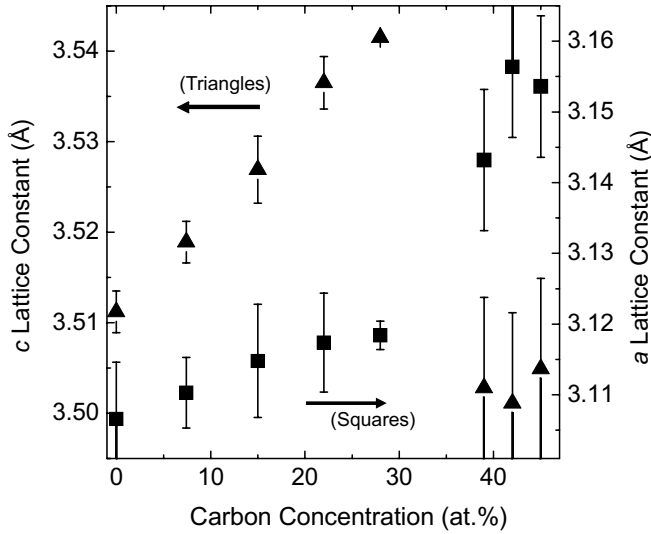


Fig. 14. The c -axis lattice constant (triangles) and a -axis lattice constant (squares) of carbon-allyed HPCVD films as a function of carbon concentration (from Ref. [95]).

the carbon is doped into the MgB_2 structure and the rest forms high resistance grain boundaries.

Carbon-allying leads to extraordinarily high H_{c2} values in the HPCVD films [47,100]. Fig. 15 shows H_{c2} vs temperature plots for a carbon-allyed HPCVD film, Nb–Ti (bulk), and Nb_3Sn (bulk) [18]. H_{c2} over 60 T at low temperatures is observed in the carbon-allyed film when the magnetic field is parallel to the ab -plane. The enhancement of H_{c2} over clean MgB_2 samples is the result of the modification of interband and intraband scattering by carbon allying [101]. The H_{c2} values for both parallel and perpendicular field directions are higher than those of the stan-

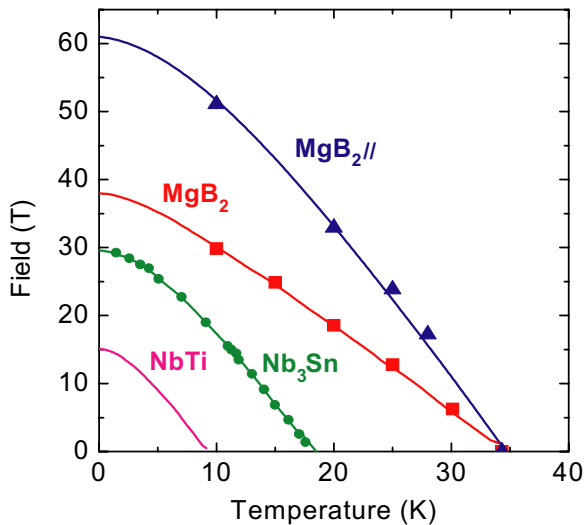


Fig. 15. H_{c2} vs temperature plots for a carbon-allyed HPCVD film, Nb–Ti (bulk), and Nb_3Sn (bulk). The triangle and square data are for the ab -planes of MgB_2 parallel and normal to the field, respectively (from Ref. [18]).

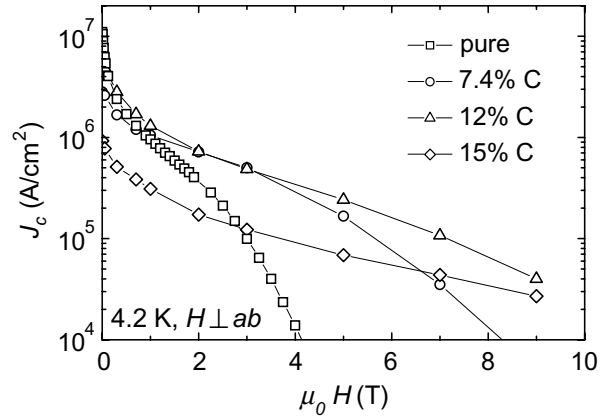


Fig. 16. J_c as a function of applied magnetic field for pure and carbon-allyed MgB_2 films of different nominal carbon contents at $T = 4.2$ K. The magnetic field direction is $H \perp ab$ (from Ref. [106]).

ard high-field materials Nb-based superconductors at all temperatures. This result is very promising for high-field applications such as in magnetic resonance imaging (MRI) [102,103]. If the operating temperature of MRI systems can be raised so that liquid helium cooling can be replaced by efficient cryocoolers, MRI systems would become lighter, of lower operation cost, more reliable, and more accessible to populations in remote locations or in developing countries [104,105]. The result in Fig. 15 demonstrates that MgB_2 could become the conductor in such MRI systems.

Carbon allying also enhances flux pinning [106]. The H_{irr} value for carbon-allyed MgB_2 film reaches ~ 45 T at low temperatures, which is considerably higher than any previously reported H_{irr} values in MgB_2 (25.4 T at 4.2 K in MgB_2 wires with SiC nanoparticle additions [107]), and much higher than those in Nb–Ti and Nb_3Sn [108]. Fig. 16 shows $J_c(H)$ for pure and carbon-allyed MgB_2 films at $T = 4.2$ K in perpendicular magnetic field [106]. The stronger pinning in the carbon-allyed MgB_2 films leads to significant improvement in the field dependence of critical current density. For the pure MgB_2 film, the self-field J_c is very high, but it drops quickly in magnetic field. When alloyed with carbon, the self-field J_c decreases due to the decrease in the current-carrying cross-section area [96]. However, the suppression of J_c by magnetic field becomes weaker and at high fields, J_c is much higher in the carbon-allyed films than in the pure MgB_2 film.

6. Polycrystalline MgB_2 films

The extraordinarily high H_{c2} of over 60 T shown in Fig. 15 was obtained in textured MgB_2 films [47]. It is important that such result can be translated into practical high-field wires or tapes. Most likely such wires or tapes will be made from polycrystalline MgB_2 materials. Using HPCVD, we have fabricated MgB_2 coated-conductor fibers, and the carbon-allyed fibers show high H_{c2} (55 T) and high H_{irr} (near 40 T) at low temperatures [48].

Fig. 17 shows SEM images of a pure MgB_2 coated-conductor fiber on a $100\ \mu\text{m}$ SiC fiber with a tungsten core. A uniform coating of the SiC fiber is found and the MgB_2 coating has a granular structure with randomly oriented crystallites. X-ray diffraction confirms that the MgB_2 coating is polycrystalline [48]. This work demonstrates that epitaxy and texture are not necessary for superb performance of MgB_2 in high magnetic fields.

The insensitivity of the properties of MgB_2 to epitaxy and texture is due to the fact that in polycrystalline MgB_2 grain boundaries are not weak links [109]. This is further demonstrated by the microwave measurement in polycrystalline HPCVD MgB_2 films on yttrium-stabilized zirconia (YSZ) substrate [49]. Fig. 18 shows the microwave surface resistance R_s at 10 GHz as a function of inverse temperature for 300 nm thick MgB_2 films on flexible YSZ substrates and c -cut sapphire single-crystals. The R_s value of the polycrystalline MgB_2 films is the same as that from the epitaxial films, and they are similar to the best result reported previously on MgB_2 films measured using the same technique [110]. The ability of polycrystalline HPCVD films to carry supercurrent is also demonstrated by Chen et al. in a microwave microstrip resonator using double-sided MgB_2 films on sapphire substrate where the two sides are connected by polycrystalline films through two holes on the substrate [111].

Polycrystalline MgB_2 films on metallic substrates have also been grown using HPCVD. For example, thick HPCVD MgB_2 films have been reported by Chen et al. on stainless steel substrates using high concentration $\text{B}_2\text{H}_6/\text{H}_2$ mixture gas [112]. In Fig. 19, our result of polycrystalline MgB_2 films on stainless steel and niobium substrates are plotted. Because the substrates are conducting and therefore form parallel conduction channels with

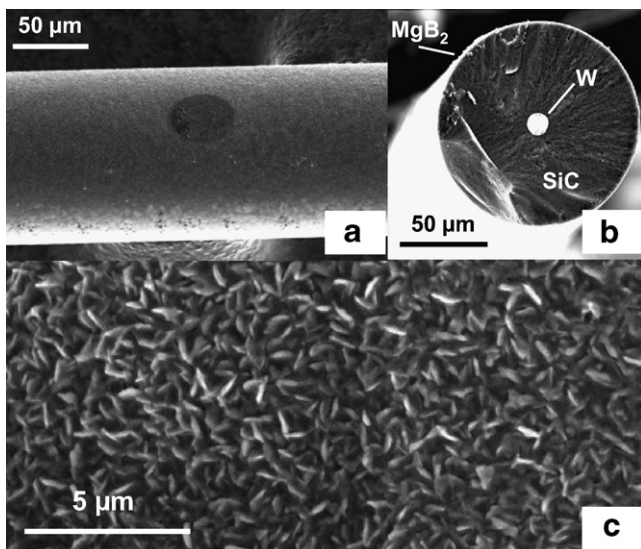


Fig. 17. (a) An SEM image of a MgB_2 coated-conductor fiber. (b) A cross-section view of the MgB_2 coated-conductor fiber. (c) A blown-up SEM image of the surface, showing elongated MgB_2 crystallites with random orientations. (from Ref. [48]).

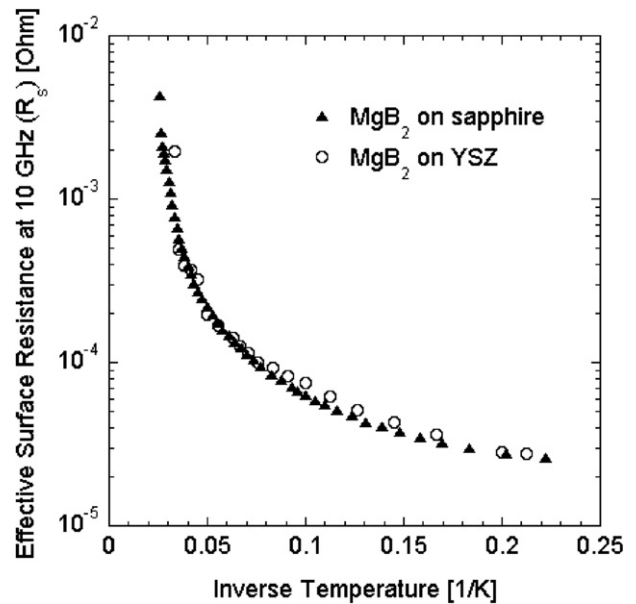


Fig. 18. Surface resistance at 10 GHz as a function of temperature for polycrystalline MgB_2 films on flexible YSZ substrates and epitaxial MgB_2 films on c -cut sapphire single-crystal, measured by a parallel plate technique (from Ref. [49]).

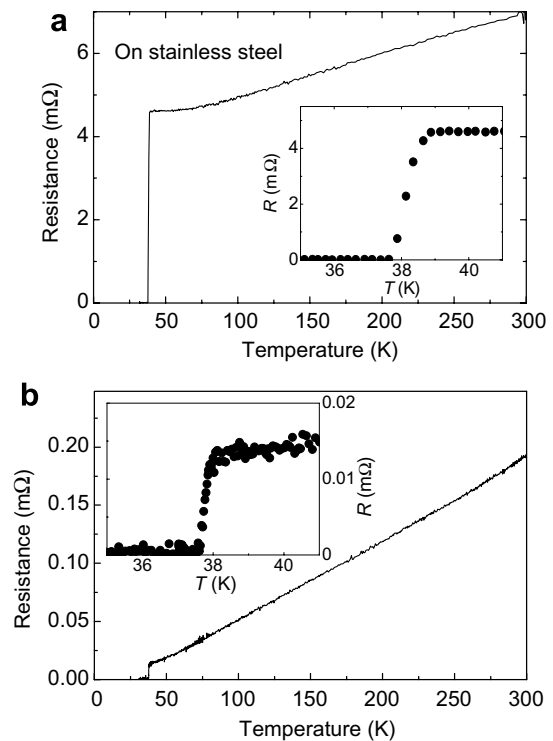


Fig. 19. Resistance vs temperature for polycrystalline MgB_2 films on (a) stainless steel and (b) niobium substrates. The insets are details near the transitions.

MgB_2 , it is difficult to extract the resistivity of MgB_2 films from the measurements. Nevertheless, superconducting transition at $\sim 38\ \text{K}$ is obtained for both substrates. As the MgB_2 coating on coated-conductor wires and tapes

or on microwave cavities are most likely on metallic substrates, these results are very encouraging.

7. Epitaxial boride heterostructures

The family of boride materials consists of a variety of structures [113] and possesses a wide range of properties from refractory highly conductive metal to semimetal, narrow-band-gap semiconductor, and wide-band-gap semiconductors [114]. Besides the two-band superconductivity in MgB_2 [6], there are extremely diversified magnetic properties in transition metal and rare-earth borides [115–117], self-healing of radiation-induced defects in some icosahedral borides [118,119], and large low-temperature Seebeck coefficient and resistivity, thus high thermoelectric figure of merit ZT , in some rare-earth hexaborides [120,121], just to name a few.

Despite these interesting properties, epitaxial thin films of borides had only been scarcely studied [122–124] before the discovery of superconductivity in MgB_2 . Since then, epitaxial films of not only MgB_2 but also other diborides such as TiB_2 [125] and ZrB_2 [126] have been deposited. We are on the verge of a completely new field of research – multifunctional epitaxial boride heterostructures. By combining the multiple functionalities of borides in epitaxial heterostructures, new physics and new devices can be studied.

Using HPCVD, we have grown MgB_2 films on pulsed-laser-deposited [22] and sputtered [16] TiB_2 films to form epitaxial $\text{MgB}_2/\text{TiB}_2$ bilayers. Fig. 20 shows structures of a $\text{MgB}_2/\text{TiB}_2$ bilayer studied by TEM. From the bright-field image in Fig. 20a we find that the TiB_2 layer exhibits a columnar grain structure. The SAED pattern in Fig. 20b shows that both TiB_2 and MgB_2 layers grow epitaxially on the SiC substrate with the c -axis normal to the substrate surface and an in-plane epitaxial relationship of $[1\bar{1}00]\text{MgB}_2\parallel[1\bar{1}00]\text{TiB}_2\parallel[1\bar{1}00]\text{SiC}$. Diffraction segments instead of spots are observed for TiB_2 , suggesting that the TiB_2 grains have both tilt and rotation. However, the MgB_2 layer on top of TiB_2 grows with high crystallinity. Fig. 20c and d show HRTEM images of the interfaces between TiB_2 and SiC substrate and between MgB_2 and TiB_2 , respectively, indicating epitaxial growth in both cases.

The epitaxial $\text{MgB}_2/\text{TiB}_2$ bilayers have been used to make planar Josephson junctions that work over 20 K [16], which are discussed in the next section. It is an excellent example of devices made possible by epitaxial boride heterostructures.

8. Josephson junctions and SQUIDs

Several types of MgB_2 Josephson junctions have been made using HPCVD films: nanobridge constrictions in epitaxial MgB_2 films [17], ion-damaged weak link planar junctions [127], planar superconductor–normal metal–superconductor (SNS) junctions using epitaxial $\text{MgB}_2/\text{TiB}_2$ bilayers [16], and MgB_2 -barrier–Pb superconductor–insulator–superconductor (SIS) trilayer junctions [60]. SQUIDs fabricated from the nanoconstrictions show stable SQUID voltage modulation up to 38.8 K [17]. A 20-junction series array made from the ion-damaged junctions shows flat giant Shapiro steps 20 times that of a single junction [127], indicating a small spread in $I_c R_n$. The trilayer MgB_2 -barrier–Pb SIS Josephson junctions made from c -axis and tilted c -axis films allow the observation of both the σ and π gaps, which have values consistent with the theoretical predictions [6]. More information can be found in the chapter by Brinkman and Rowell in this issue [50].

Here we discuss in more detail the planar SNS Josephson junctions using epitaxial $\text{MgB}_2/\text{TiB}_2$ bilayers, where TiB_2 serves as the barrier material [16,128]. TiB_2 is a conductive material with excellent mechanical, tribological, chemical, and thermal properties [129]. On a bilayer film of $\text{MgB}_2/\text{TiB}_2$, MgB_2 was locally removed to create a gap of ~ 50 nm by e-beam lithography and ion milling or by focused ion beam, and the Josephson coupling is established through the TiB_2 film across the gap by proximity effect. Fig. 21 shows I - V characteristics of a $\text{MgB}_2/\text{TiB}_2/\text{MgB}_2$ junction without and with 29.5 GHz microwave radiation of different powers measured at $T = 28$ K. The junction without RF radiation exhibits I - V curves in good agreement with the resistively shunted junction (RSJ) model. Clear ac Josephson effect is observed with Shapiro

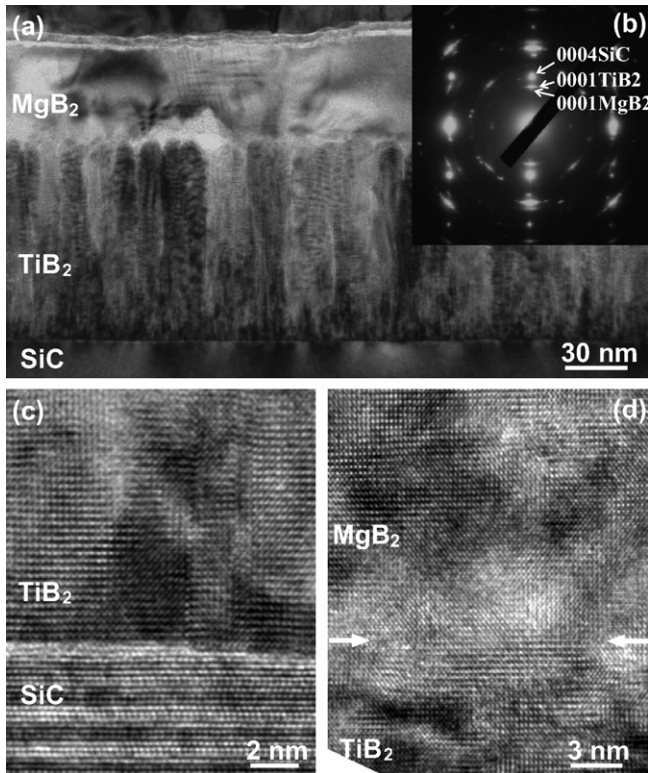


Fig. 20. (a) Bright-field TEM image of a $\text{MgB}_2/\text{TiB}_2$ bilayer. (b) SAED pattern collected from an area containing all the layers. (c) HRTEM image of the TiB_2/SiC substrate interface. (d) HRTEM image of the $\text{MgB}_2/\text{TiB}_2$ interface. The arrows indicate the interface.

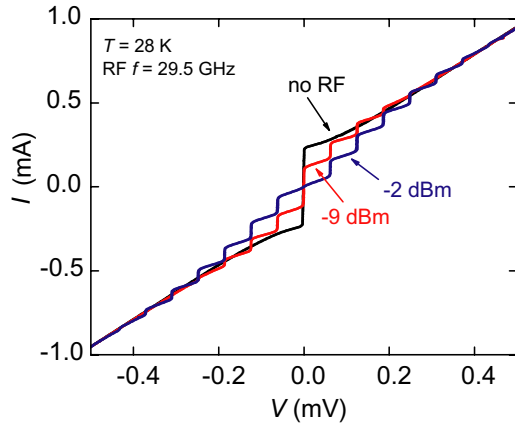


Fig. 21. Current–voltage characteristics of a planar $\text{MgB}_2/\text{TiB}_2/\text{MgB}_2$ junction at 28 K with and without applied 29.5 GHz microwave radiation (from Ref. [16]).

steps at voltages $V_n = nhf/2e$, where f is the microwave frequency, h is the plank constant, and $n = 0, 1, 2, \dots$ is the order of the steps. The step-height vs microwave voltage across the junction agrees with the current-source model quantitatively. The $\text{MgB}_2/\text{TiB}_2$ heterostructure allowed successful fabrication of high quality MgB_2 Josephson junctions that work well above 20 K.

Washer-type dc SQUIDs with inner square dimension of $30 \mu\text{m} \times 30 \mu\text{m}$ and outer square dimension of $3.5 \text{mm} \times 3.5 \text{mm}$ were made using the planar $\text{MgB}_2/\text{TiB}_2/\text{MgB}_2$ junctions. Fig. 22 shows the dc voltage across such a dc SQUID at different temperatures under applied magnetic field perpendicular to the film surface generated by an uncalibrated coil. Large voltage modulation is observed in the SQUID at temperatures above 20 K. The slow change in the voltage may be due to the difference

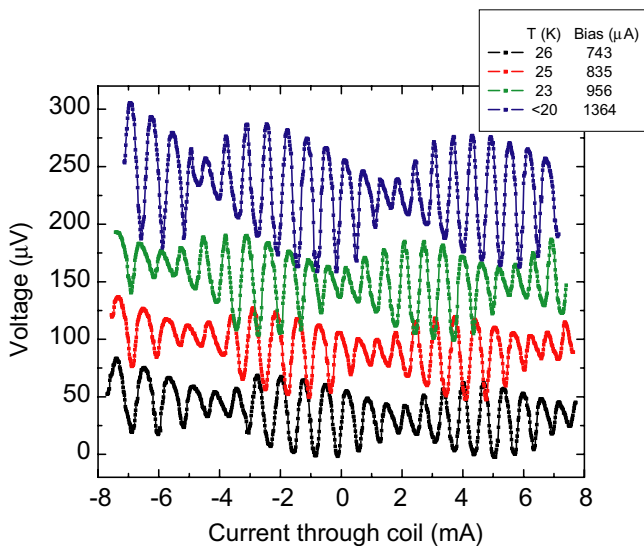


Fig. 22. The magnetic field dependence of dc voltage across a MgB_2 dc SQUID at different temperatures. The dc bias currents are chosen to maximize the voltage modulation amplitude.

in the properties of the two $\text{MgB}_2/\text{TiB}_2/\text{MgB}_2$ junctions in the SQUID.

One important issue for device applications of MgB_2 is its stability, in the ambient atmosphere, moisture, solvents, or water. We have found that the HPCVD films degrade easily in water [130]. When exposed to water, T_c decreases and resistivity increases, and the film becomes thinner and turns into a transparent insulating material [130]. Preliminary X-ray photo-emission spectroscopy (XPS) study found that there is only a very thin (5–10 Å) MgB_xO_y or $\text{Mg}(\text{OH})_2$ layer at the film surface on top of the MgB_2 film bulk. Thus there is little protection at the film surface for MgB_2 from reaction with water. This has been corroborated by the point-contact spectroscopy measurement of Park and Greene, who found that the point-contact spectrum on HPCVD films are Andreev-reflection-like, indicating a metallic surface, while the spectrum on films deposited by reactive co-evaporation is tunneling-like, indicating a surface with a tunnel barrier layer [131]. MgB_2 films by reactive co-evaporation degrade much more slowly in water [42], likely due to this protection layer.

9. Concluding remarks

HPCVD has shown to be a very effective technique for MgB_2 thin films. The scope of its impact has been remarkably broad: from the cleanest MgB_2 material to the highest H_{c2} values in carbon-alloyed films; from the studies of new physics due to the two-band nature of MgB_2 to the investigations of practical applications such as in MgB_2 coated conductors; and from superconducting digital circuits using Josephson junctions to cryogen-free superconducting magnets for MRI systems. There is no doubt that the importance of the HPCVD technique to MgB_2 research and applications will continue to grow.

The HPCVD technique is still in its early development stage. The initial setup shown in Fig. 2 does not allow independent control over the substrate and Mg source temperatures. As a result, whenever the substrate temperature is changed, the Mg vapor pressure changes as well, limiting the ranges of the growth parameters [44,132]. In the new generation of HPCVD systems, the Mg source and substrate heater are separated and controlled independently [133]. In the setup shown in Fig. 2, the size of the uniform MgB_2 films is limited by the complex Mg vapor distribution and B_2H_6 flow near the substrate. Further, the initial HPCVD system is not capable of *in situ* deposition of multilayers of different materials. These limitations will be addressed in the next generation HPCVD systems. In addition, special configuration HPCVD systems need to be designed for coating long-length coated-conductor wires or tapes and non-flat surfaces such as in microwave cavities.

One area that has not been fully investigated by HPCVD but important for basic and applied research of MgB_2 is the doping of MgB_2 films. When a precursor can be found that contains the dopant and decomposes at the

substrate to release the dopant element, such as $(\text{MeCp})_2\text{Mg}$ used in the carbon-alloyed films, doping can be easily achieved in HPCVD. However, if such precursor is not found doping can be difficult to implement by HPCVD. So far, only carbon has been doped to the MgB_2 films by HPCVD using $(\text{MeCp})_2\text{Mg}$. It is of great interest to use other carbon-containing precursors, such as trimethylboron, for carbon doping to study possible different microstructures and properties in the films. Doping of MgB_2 with Al, Mn [134], and Ti [135] is also of interest.

Before concluding, it is useful to note again that the most critical attributes of the HPCVD technique for its success are its ability to provide a sufficiently high Mg vapor pressure, the high purity sources of Mg and B, and a clean oxygen-free environment to grow films. As long as they are maintained, HPCVD can have many variations, even in combination with other deposition approaches. For example, the reactive co-evaporation technique [42], which employs alternating B deposition and reaction in Mg vapor repeated in very thin layer scales, has successfully produced *in situ* MgB_2 with good properties. It is conceivable that such a process can be fashioned in an HPCVD system. A step further in this direction is the technique to deposit one single B layer followed by a high-temperature reaction in Mg vapor [23,24]. Chemical vapor deposition of B films using B_2H_6 as precursor has been used in such a process [29,136]. This may be a viable process for coating objects such as the inner surface of microwave cavities.

Acknowledgements

We would like to thank our many colleagues and collaborators, whose published works are quoted in this paper. This work is supported in part by ONR under Grant Nos. N00014-00-1-0294 (XXX), N00014-07-1-0079 (XXX), and N0014-01-1-0006 (JMR), by NSF under Grant Nos. DMR-0306746 (XXX and JMR), DMR-0405502 (QL), DMR-0514592 (ZKL), DMR-0507146 (DGS and XXX), and DMR-9871177 (XQP), and by AFOSR under Grant No. FDFA9550-05-1-0436 (RCD).

References

- [1] J. Nagamatsu, N. Nakagawa, T. Muranaka, Y. Zenitani, J. Akimitsu, *Nature* (London) 410 (2001) 63.
- [2] S.L. Bud'ko, G. Lapertot, C. Petrovic, C.E. Cunningham, N. Anderson, P.C. Canfield, *Phys. Rev. Lett.* 86 (2001) 1877.
- [3] J. Kortus, I.I. Mazin, K.D. Belashchenko, V.P. Antropov, L.L. Boyer, *Phys. Rev. Lett.* 86 (2001) 4656.
- [4] A.Y. Liu, I.I. Mazin, J. Kortus, *Phys. Rev. Lett.* 87 (2001) 087005.
- [5] J.M. An, W.E. Pickett, *Phys. Rev. Lett.* 86 (2001) 4366.
- [6] H.J. Choi, D. Roundy, H. Sun, M.L. Cohen, S.G. Louie, *Nature* (London) 418 (2002) 758.
- [7] P.C. Canfield, G. Crabtree, *Phys. Today* 56 (3) (2003) 34.
- [8] W. Pickett, *Nature* (London) 418 (2002) 733.
- [9] Q. Li, B.T. Liu, Y.F. Hu, J. Chen, H. Gao, L. Shan, H.H. Wen, A. Pogrebnnyakov, J.M. Redwing, X.X. Xi, *Phys. Rev. Lett.* 96 (2006) 167003.
- [10] A. Gurevich, V. Vinokur, *Phys. Rev. Lett.* 90 (2003) 047004.
- [11] A. Gurevich, V. Vinokur, *Phys. Rev. Lett.* 97 (2006) 137003.
- [12] S.G. Sharapov, V. Gusynin, H. Beck, *Eur. Phys. J.* B30 (2002) 45.
- [13] D.F. Agterberg, E. Demler, B. Janko, *Phys. Rev. B* 66 (2002) 214507.
- [14] J. Rowell, *Nat. Mater.* 1 (2002) 5.
- [15] H.J.M. ter Brake, G.F.M. Wiegerinck, *Cryogenics* 42 (2002) 705.
- [16] K. Chen, Y. Cui, Q. Li, X.X. Xi, S.A. Cybart, R.C. Dynes, X. Weng, E.C. Dickey, J.M. Redwing, *Appl. Phys. Lett.* 88 (2006) 222511.
- [17] D. Mijatovic, A. Brinkman, D. Veldhuis, H. Hilgenkamp, H. Rogalla, G. Rijnders, D.H.A. Blank, A.V. Pogrebnnyakov, J.M. Redwing, S.Y. Xu, Q. Li, X.X. Xi, *Appl. Phys. Lett.* 87 (2005) 192505.
- [18] Y. Iwasa, D.C. Larbalestier, M. Okada, R. Penco, M. Sumption, X. Xi, *IEEE Trans. Appl. Supercond.* 16 (2006) 1457.
- [19] J. Bascuñán, H. Lee, E.S. Bobrov, S. Hahn, Y. Iwasa, M. Tomsic, M. Rindfleisch, *IEEE Trans. Appl. Supercond.* 16 (2006) 1427.
- [20] R. Vaglio, *Particle Accelerators* 61 (1998) 391.
- [21] E.W. Collings, M.D. Sumption, T. Tajima, *Supercond. Sci. Technol.* 17 (2004) S595.
- [22] X.X. Xi, A.V. Pogrebnnyakov, X.H. Zeng, J.M. Redwing, S.Y. Xu, Q. Li, Z.-K. Liu, J. Lettieri, V. Vaithyanathan, D.G. Schlom, H.M. Christen, H.Y. Zhai, A. Goyal, *Supercond. Sci. Technol.* 17 (2004) S196.
- [23] W.N. Kang, H.-J. Kim, E.-M. Choi, C.U. Jung, S.-I. Lee, *Science* 292 (2001) 1521.
- [24] C.B. Eom, M.K. Lee, J.H. Choi, L. Belenky, X. Song, L.D. Cooley, M.T. Naus, S. Patnaik, J. Jiang, M.O. Rikel, A.A. Polyanskii, A. Gurevich, X.Y. Cai, S.D. Bu, S.E. Babcock, E.E. Hellstrom, D.C. Larbalestier, N. Rogado, K.A. Regan, M.A. Hayward, T. He, J.S. Slusky, K. Inumaru, M. Haas, R.J. Cava, *Nature* (London) 411 (2001) 558.
- [25] C. Ferdeghini, V. Ferrando, G. Grassano, W. Ramadan, E. Bellingeri, V. Braccini, D. Marré, P. Manfrinetti, A. Palenzona, F. Borgatti, R. Felici, T.-L. Lee, *Supercond. Sci. Technol.* 14 (2001) 952.
- [26] A. Berenov, Z. Lockman, X. Qi, J.L. MacManus-Driscoll, Y. Bugoslavsky, L.F. Cohen, M.-H. Jo, N.A. Stelmashenko, V.N. Tsaneva, M. Kambara, N.H. Babu, D.A. Cardwell, M.G. Blamire, *Appl. Phys. Lett.* 79 (2001) 4001.
- [27] R. Vaglio, M.G. Maglione, R. Di Capua, *Supercond. Sci. Technol.* 15 (2002) 1236.
- [28] S.H. Moon, J.H. Yun, H.N. Lee, J.I. Kye, H.G. Kim, W. Chung, B. Oh, *Appl. Phys. Lett.* 79 (2001) 2429.
- [29] X.H. Fu, D.S. Wang, Z.P. Zhang, J. Yang, *Physica C* 377 (2002) 407.
- [30] D.H.A. Blank, H. Hilgenkamp, A. Brinkman, D. Mijatovic, G. Rijnders, H. Rogalla, *Appl. Phys. Lett.* 79 (2001) 394.
- [31] S.R. Shinde, S.B. Ogale, R.L. Greene, T. Venkatesan, P.C. Canfield, S. Bud'ko, G. Lapertot, C. Petrovic, *Appl. Phys. Lett.* 79 (2001) 227.
- [32] H. Christen, H. Zhai, C. Cantoni, M. Paranthaman, B. Sales, C. Rouleau, D. Norton, D. Christen, D. Lowndes, *Physica C* 353 (2001) 157.
- [33] X.H. Zeng, A. Sukiasyan, X.X. Xi, Y.F. Hu, E. Wertz, Q. Li, W. Tian, H.P. Sun, X.Q. Pan, J. Lettieri, D.G. Schlom, C.O. Brubaker, Z.-K. Liu, Q. Li, *Appl. Phys. Lett.* 79 (2001) 1840.
- [34] S.N. Ermolov, M.V. Indenbom, A.N. Rossolenko, I.K. Bdikin, L.S. Uspenskaya, N.S. Stepanov, V.G. Glebovskii, *JETP Lett.* 73 (2001) 557.
- [35] A. Plecenik, L. Satrapinsky, P. Kúš, Š. Gaži, Š. Beňačka, I. Vávra, I. Kostič, *Physica C* 363 (2001) 224.
- [36] J. Kim, R.K. Singh, N. Newman, J.M. Rowell, *IEEE Trans. Appl. Supercond.* 13 (2003) 3238.
- [37] K. Ueda, M. Naito, *Appl. Phys. Lett.* 79 (2001) 2046.
- [38] W. Jo, J.-U. Huh, T. Ohnishi, A.F. Marshall, M.R. Beasley, R.H. Hammond, *Appl. Phys. Lett.* 80 (2002) 3563.
- [39] A.J.M. van Erven, T.H. Kim, M. Muenzenberg, J.S. Moodera, *Appl. Phys. Lett.* 81 (2002) 4982.

- [40] A. Saito, A. Kawakami, H. Shimakage, Z. Wang, *Jpn. J. Appl. Phys.* 41 (2002) L127.
- [41] R. Schneider, J. Geerk, F. Ratzel, G. Linker, A. Zaitsev, *Appl. Phys. Lett.* 85 (2004) 5290.
- [42] B.H. Moeckly, W.S. Ruby, *Supercond. Sci. Tech.* 19 (2006) L21.
- [43] X.H. Zeng, A.V. Pogrebnnyakov, A. Kotcharov, J.E. Jones, X.X. Xi, E.M. Lysczek, J.M. Redwing, S.Y. Xu, Q. Li, J. Lettieri, D.G. Schlom, W. Tian, X.Q. Pan, Z.K. Liu, *Nat. Mater.* 1 (2002) 35.
- [44] X.X. Xi, X.H. Zeng, A.V. Pogrebnnyakov, S.Y. Xu, Q. Li, Y. Zhong, C.O. Brubaker, Z.-K. Liu, E.M. Lysczek, J.M. Redwing, J. Lettieri, D.G. Schlom, W. Tian, X.Q. Pan, *IEEE Trans. Appl. Supercond.* 13 (2003) 3233.
- [45] X.H. Zeng, A.V. Pogrebnnyakov, M.H. Zhu, J.E. Jones, X.X. Xi, S.Y. Xu, E. Wertz, Q. Li, J.M. Redwing, J. Lettieri, V. Vaithyanathan, D.G. Schlom, Z.K. Liu, O. Trithaveesak, J. Schubert, *Appl. Phys. Lett.* 82 (2003) 2097.
- [46] A.V. Pogrebnnyakov, D.A. Tenne, A. Soukiassian, X.X. Xi, J.M. Redwing, V. Vaithyanathan, D.G. Schlom, S.Y. Xu, Q. Li, M.D. Johannes, D. Kasinathan, W.E. Pickett, *Phys. Rev. Lett.* 93 (2004) 147006.
- [47] V. Braccini, A. Gurevich, J. Giencke, M. Jewell, C. Eom, D. Larbalestier, A. Pogrebnnyakov, Y. Cui, B.T. Liu, Y.F. Hu, J.M. Redwing, Q. Li, X.X. Xi, R. Singh, R. Gandikota, J. Kim, B. Wilkens, N. Newmann, J. Rowell, B. Moeckly, V. Ferrando, C. Tarantini, D. Marré, M. Putti, C. Ferdeghini, R. Vaglio, E. Haanappel, *Phys. Rev. B* 71 (2005) 012504.
- [48] V. Ferrando, P. Orgiani, A.V. Pogrebnnyakov, J. Chen, Q. Li, J.M. Redwing, X.X. Xi, J.E. Giencke, C.B. Eom, Q.-R. Feng, J.B. Betts, C.H. Mielke, *Appl. Phys. Lett.* 87 (2005) 252509.
- [49] A.V. Pogrebnnyakov, E. Maertz, R.H.T. Wilke, Q. Li, A. Soukiassian, D.G. Schlom, J.M. Redwing, A. Findikoglu, X.X. Xi, Polycrystalline MgB₂ films on flexible YSZ substrates grown by hybrid physical–chemical vapor deposition, *IEEE Trans. Appl. Supercond.*, submitted for publication.
- [50] A. Brinkman, J.M. Rowell, Epitaxial MgB₂ tunnel junctions and SQUIDS, *Physica C*, this issue.
- [51] Z.K. Liu, D.G. Schlom, Q. Li, X.X. Xi, *Appl. Phys. Lett.* 78 (2001) 3678.
- [52] Z.Y. Fan, D.G. Hinks, N. Newman, J.M. Rowell, *Appl. Phys. Lett.* 79 (2001) 87.
- [53] R.A. Ribeiro, S.L. Bud'ko, C. Petrovic, P.C. Canfield, *Physica C* 384 (2003) 227.
- [54] D.R. Lamborn, D.W. Snyder, X.X. Xi, J.M. Redwing, Modeling studies of the chemical vapor deposition of boron films from B₂H₆, *J. Cryst. Growth*, in press.
- [55] S.D. Bu, D.M. Kim, J.H. Choi, J. Giencke, S. Patnaik, L. Cooley, E.E. Hellstrom, D.C. Larbalestier, C.B. Eom, J. Lettieri, D.G. Schlom, W. Tian, X. Pan, *Appl. Phys. Lett.* 81 (2002) 1851.
- [56] W. Tian, X.Q. Pan, S.D. Bu, D.M. Kim, J.H. Choi, S. Patnaik, C.B. Eom, *Appl. Phys. Lett.* 81 (2002) 685.
- [57] J.S. Wu, N. Jiang, B. Jiang, J.C.H. Spence, A.V. Pogrebnnyakov, J.M. Redwing, X.X. Xi, *Appl. Phys. Lett.* 85 (2004) 1155.
- [58] A. Brinkman, A.A. Golubov, H. Rogalla, O.V. Dolgov, J. Kortus, Y. Kong, O. Jepsen, O.K. Andersen, *Phys. Rev. B* 65 (2002) 180517.
- [59] M. Iavarone, G. Karapetrov, A. Menzel, V. Komanicky, H. You, W.K. Kwok, P. Orgiani, V. Ferrando, X.X. Xi, *Appl. Phys. Lett.* 87 (2005) 242506.
- [60] Y. Cui, K. Chen, Q. Li, X.X. Xi, J.M. Rowell, *Appl. Phys. Lett.* 89 (2006) 202513.
- [61] A.V. Pogrebnnyakov, J.M. Redwing, J.E. Jones, X.X. Xi, S.Y. Xu, Q. Li, V. Vaithyanathan, D.G. Schlom, *Appl. Phys. Lett.* 82 (2003) 4319.
- [62] S. Lee, *Physica C* 385 (2003) 31.
- [63] P.C. Canfield, D.K. Finnemore, S.L. Bud'ko, J.E. Ostenson, G. Lapertot, C.E. Cunningham, C. Petrovic, *Phys. Rev. Lett.* 86 (2001) 2423.
- [64] I. Pallecchi, M. Monni, C. Ferdeghini, V. Ferrando, M. Putti, C. Tarantini, E. Galleani D'Agliano, *Eur. Phys. J. B* 52 (2006) 171.
- [65] V. Ferrando, I. Pallecchi, C. Tarantini, D. Marré, M. Putti, F. Gatti, H.U. Aebbersold, E. Lehmann, E. Haanappel, I. Sheikin, X.X. Xi, P. Orgiani, C. Ferdeghini, Systematic study of disorder induced by neutron irradiation in MgB₂ thin films, *J. Appl. Phys.* 101 (2007) 043903.
- [66] D.C. Larbalestier, A. Gurevich, D.M. Feldmann, A.A. Polyanskii, *Nature (London)* 414 (2001) 368.
- [67] J.A. Floro, E. Chason, R.C. Cammarata, D.J. Srolovitz, *MRS Bull.* 27 (1) (2002) 19.
- [68] R. Koch, *J. Phys.: Condens. Matter* 6 (1994) 9519.
- [69] J.E. Moussa, M.L. Cohen, *Phys. Rev. B* 74 (2006) 094520.
- [70] C. Kittel, *Quantum Theory of Solids*, John Wiley & Sons, Inc, New York, 1993.
- [71] J. Callaway, *Quantum Theory of the Solid State*, Academic Press, New York, 1976.
- [72] J.M. Ziman, *Electrons and Phonons*, Classics Series, Oxford University Press, New York, 2001.
- [73] I.I. Mazin, O.K. Andersen, O. Jepsen, O.V. Dolgov, J. Kortus, A.A. Golubov, A.B. Kuzmenko, D. van der Marel, *Phys. Rev. Lett.* 89 (2002) 107002.
- [74] A.J. Leggett, *Prog. Theor. Phys.* 36 (1966) 901.
- [75] A.J. Leggett, *Rev. Mod. Phys.* 76 (2004) 999.
- [76] E. Babaev, *Phys. Rev. Lett.* 89 (2002) 067001.
- [77] A.E. Koshelev, A.A. Golubov, *Phys. Rev. Lett.* 92 (2004) 107008.
- [78] B.B. Jin, T. Dahm, C. Iniotakis, A.I. Gubin, E.-M. Choi, H.J. Kim, S.-I. Lee, W.N. Kang, S.F. Wang, Y.L. Zhou, A.V. Pogrebnnyakov, J.M. Redwing, X.X. Xi, N. Klein, *Supercond. Sci. Technol.* 18 (2005) L1.
- [79] B.B. Jin, T. Dahm, A.I. Gubin, E.-M. Choi, H.-J. Kim, S.-I. Lee, W. Kang, N. Klein, *Phys. Rev. Lett.* 91 (2003) 127006.
- [80] M. Putti, M. Affronte, C. Ferdeghini, P. Manfrinetti, C. Tarantini, E. Lehmann, *Phys. Rev. Lett.* 96 (2006) 077003.
- [81] D.E. Oates, S.-H. Park, D. Agassi, G. Koren, K. Irgmaier, *IEEE Trans. Appl. Supercond.* 15 (2005) 3589.
- [82] T. Dahm, N. Schopohl, *Phys. Rev. Lett.* 91 (2003) 017001.
- [83] G. Cifariello, M. Aurino, E.D. Gennaro, G. Lamura, P. Orgiani, J.-C. Villégier, X.X. Xi, A. Andreone, *Appl. Phys. Lett.* 88 (2006) 142510.
- [84] N. Klein, *Rep. Prog. Phys.* 65 (2002) 1387.
- [85] B.B. Jin, P. Kuzel, F. Kadlec, T. Dahm, J.M. Redwing, A.V. Pogrebnnyakov, X.X. Xi, N. Klein, *Appl. Phys. Lett.* 87 (2005) 092503.
- [86] S. Jin, H. Mavoori, C. Bower, R.B. van Dover, *Nature (London)* 411 (2001) 563.
- [87] T.H. Johansen, M. Baziljevich, D.V. Shantsev, P.E. Goa, Y.M. Galperin, W.N. Kang, H.J. Kim, E.M. Choi, M.-S. Kim, S.I. Lee, *Europhys. Lett.* 59 (2002) 599.
- [88] R.G. Mints, A.L. Rakhmanov, *Rev. Mod. Phys.* 53 (1981) 551.
- [89] Z.X. Ye, Q. Li, Y.F. Hu, A.V. Pogrebnnyakov, Y. Cui, X.X. Xi, J.M. Redwing, Q. Li, *Appl. Phys. Lett.* 85 (2004) 5284.
- [90] Z.X. Ye, Q. Li, Y.F. Hu, A.V. Pogrebnnyakov, Y. Cui, X.X. Xi, J.M. Redwing, Q. Li, *IEEE Trans. Appl. Supercond.* 15 (2005) 3273.
- [91] S.R. Shinde, S.B. Ogale, J. Higgins, R.J. Choudhary, V.N. Kulkarni, T. Venkatesan, H. Zheng, R. Ramesh, A.V. Pogrebnnyakov, S.Y. Xu, Q. Li, X.X. Xi, J.M. Redwing, D. Kanjilal, *Appl. Phys. Lett.* 84 (2004) 2352.
- [92] R. Gandikota, R.K. Singh, J. Kim, B. Wilkens, N. Newman, J.M. Rowell, A.V. Pogrebnnyakov, X.X. Xi, J.M. Redwing, S.Y. Xu, Q. Li, *Appl. Phys. Lett.* 86 (2005) 012508.
- [93] R. Gandikota, R.K. Singh, J. Kim, B. Wilkens, N. Newman, J.M. Rowell, A.V. Pogrebnnyakov, X.X. Xi, J.M. Redwing, S.Y. Xu, Q. Li, B.H. Moeckly, *Appl. Phys. Lett.* 87 (2005) 072507.
- [94] A. Gurevich, S. Patnaik, V. Braccini, K.H. Kim, C. Mielke, X. Song, L.D. Cooley, S.D. Bu, D.M. Kim, J.H. Choi, L.J. Belenky, J. Giencke, M.K. Lee, W. Tian, X. Pan, A. Siri, E.E. Hellstrom, C.B. Eom, D. Larbalestier, *Supercond. Sci. Technol.* 17 (2004) 278.
- [95] A.V. Pogrebnnyakov, X.X. Xi, J.M. Redwing, V. Vaithyanathan, D.G. Schlom, A. Soukiassian, S.B. Mi, C.L. Jia, J. Giencke, C.B.

- Eom, J. Chen, Y.F. Hu, Y. Cui, Q. Li, Appl. Phys. Lett. 85 (2004) 2017.
- [96] A.V. Pogrebnnyakov, J.M. Redwing, J.E. Giенcke, C.B. Eom, V. Vaithyanathan, D.G. Schlom, A. Soukiassian, S.B. Mi, C.L. Jia, J. Chen, Y.F. Hu, Y. Cui, Q. Li, X.X. Xi, IEEE Trans. Appl. Supercond. 15 (2005) 3321.
- [97] S. Lee, T. Masui, A. Yamamoto, H. Uchiyama, S. Tajima, Physica C 397 (2003) 7.
- [98] R.H.T. Wilke, S.L. Bud'ko, P.C. Canfield, D.K. Finnemore, R.J. Suplinskas, S.T. Hannahs, Phys. Rev. Lett. 92 (2004) 217003.
- [99] D.A. Tenne, X.X. Xi, A.V. Pogrebnnyakov, J.M. Redwing, Phys. Rev. B 71 (2005) 132512.
- [100] C. Ferdeghini, V. Ferrando, C. Tarantini, E. Bellingeri, G. Grasso, A. Malagoli, D. Marré, M. Putti, P. Manfrinetti, A. Pogrebnnyakov, J.M. Redwing, X.X. Xi, R. Felici, E. Haanappel, IEEE Trans. Appl. Supercond. 15 (2005) 3234.
- [101] A. Gurevich, Phys. Rev. B 67 (2003) 184515.
- [102] G. Morrow, IEEE Trans. Appl. Supercond. 10 (2000) 744.
- [103] Committee on Opportunities in High Magnetic Field Science, Solid State Sciences Committee, National Research Council, Opportunities in High Magnetic Field Science, The National Academies Press, Washington, DC, 2005.
- [104] E.T. Laskaris, Superconductive magnetic resonance magnets without cryogenics, US Patent 4,924,198.
- [105] B.X. Xu, S. Schnurer, K. Obasih, M. Mruzek, O. Ige, R. Lochner, J. Helbing, D. Mantone, IEEE Trans. Magn. 32 (1996) 2637.
- [106] J. Chen, V. Ferrando, P. Orgiani, A.V. Pogrebnnyakov, R.H.T. Wilke, J.B. Betts, C.H. Mielke, J.M. Redwing, X.X. Xi, Q. Li, Phys. Rev. B 74 (2006) 174511.
- [107] M.D. Sumption, M. Bhatia, M. Rindfiesch, M. Tomsic, S. Soltanian, S.X. Dou, E.W. Collings, Appl. Phys. Lett. 86 (2005) 092507.
- [108] M. Suenaga, A.K. Ghosh, Y. Xu, D.O. Welch, Phys. Rev. Lett. 66 (1991) 1777.
- [109] D.C. Larbalestier, L.D. Cooley, M.O. Rikel, A.A. Polyanskii, J. Jiang, S. Patnaik, X.Y. Cai, D.M. Feldmann, A. Gurevich, A.A. Squitieri, M.T. Naus, C.B. Eom, E.E. Hellstrom, R.J. Cava, K.A. Regan, N. Rogado, M.A. Hayward, T. He, J.S. Slusky, P. Khalifah, K. Inumaru, M. Haas, Nature (London) 410 (2001) 186.
- [110] B.H. Moeckly, K.E. Kihlstrom, A.T. Findikoglu, D.E. Oates, IEEE Trans. Appl. Supercond. 15 (2005) 3308.
- [111] L.P. Chen, L.L. Ding, Q.R. Feng, G.C. Xiong, Y.F. Wang, S. Luo, X.Q. Zhang, Y.S. He, Appl. Phys. Lett. 88 (2006) 262502.
- [112] C.P. Chen, Q.R. Feng, Z.Z. Gan, G.C. Xiong, J. Xu, Y.F. Liu, L.W. Kong, L. Li, Z. Jia, J.P. Guo, C.G. Zhuang, L.L. Ding, L.P. Chen, F. Li, K.C. Zhang, Chinese Sci. Bull. 50 (2005) 719.
- [113] J. Etourneau, P. Hagenmuller, Phil. Mag. B 52 (1985) 589.
- [114] S. Kück, H. Werheit, in: O. Madelung (Ed.), LANDOLT-BÖRNSTEIN: Numerical Data and Functional Relationships in Science and Technology, New Series, vol. III/41D, Springer-Verlag, Berlin, 2000.
- [115] B.T. Matthias, T.H.G. Amd, K. Andres, E. Corenzwit, G.W. Hull, J.P. Maita, Science 159 (1968) 530.
- [116] T.H. Geballe, B.T. Matthias, K. Andres, J.P. Maita, A.S. Cooper, E. Corenzwit, Science 160 (1968) 1443.
- [117] K.H.J. Buschow, in: V.I. Matkovich (Ed.), Boron and Refractory Borides, Springer-Verlag, New York, 1977, p. 494.
- [118] M. Carrard, D. Emin, L. Zuppiroli, Phys. Rev. B 51 (1995) 11270.
- [119] T.L. Aselage, D. Emin, Beta cell device using icosahedral boride compounds, US Patent No. 6,479,919.
- [120] S.R. Harutyunyan, V.H. Vardanyan, A.S. Kuzanyan, V.R. Nikoghosyan, S. Kunii, K. Winzer, K.S. Wood, A.M. Gulian, Appl. Phys. Lett. 87 (2005) 194114.
- [121] A.S. Kuzanyan, S.R. Harutyunyan, V.O. Vardanyan, G.R. Badalyan, V.A. Petrosyan, V.S. Kuzanyan, S.I. Petrosyan, V.E. Karapetyan, K.S. Wood, H.-D. Wu, A.M. Gulian, J. Solid State Chem. 179 (2006) 2862.
- [122] M. Belyansky, M. Trenary, Chem. Mater. 9 (1997) 403.
- [123] J.R. Michael, T.L. Aselage, D. Emin, P.G. Kotula, J. Mater. Res. 20 (2005) 3004.
- [124] Z. Xu, J.H. Edgar, S. Speakman, J. Crystal Growth 293 (2006) 162.
- [125] H.Y. Zhai, H.M. Christen, C. Cantoni, A. Goyal, D.H. Lowndes, Appl. Phys. Lett. 80 (2002) 1963.
- [126] V. Ferrando, C. Tarantini, E. Bellingeri, P. Manfrinetti, I. Pallecchi, D. Marré, O. Plantevin, M. Putti, R. Felici, C. Ferdeghini, Supercond. Sci. Technol. 17 (2004) 1434.
- [127] S.A. Cybart, K. Chen, Y. Cui, Q. Li, X.X. Xi, R.C. Dynes, Appl. Phys. Lett. 88 (2006) 012509.
- [128] K. Chen, Y. Cui, Q. Li, X.X. Xi, Study of planar MgB₂/TiB₂/MgB₂ Josephson junctions using the proximity effect SNS model, IEEE Trans. Appl. Supercond., submitted for publication.
- [129] R.G. Munro, J. Res. Natl. Inst. Stand. Technol. 105 (2000) 709.
- [130] Y. Cui, J.E. Jones, A. Beckley, R. Donovan, D. Lishego, E. Maertz, A.V. Pogrebnnyakov, P. Orgiani, J.M. Redwing, X.X. Xi, IEEE Trans. Appl. Supercond. 15 (2005) 224.
- [131] W.K. Park, L.H. Greene, Rev. Sci. Instrum. 77 (2006) 023905.
- [132] B.T. Liu, X.X. Xi, V. Vaithyanathan, D.G. Schlom, IEEE Trans. Appl. Supercond. 15 (2005) 3249.
- [133] D.R. Lamborn, R.H.T. Wilke, D.W. Snyder, X.X. Xi, J.M. Redwing, Dual-heater reactor design for hybrid physical-chemical vapor deposition of MgB₂ thin films, IEEE Trans. Appl. Supercond., submitted for publication.
- [134] R.J. Cava, H.W. Zandbergen, K. Inumaru, Physica C 385 (2003) 8.
- [135] Y. Zhao, D.X. Huang, Y. Feng, C.H. Cheng, T. Machi, N. Koshizuka, M. Murakami, Appl. Phys. Lett. 80 (2002) 1640.
- [136] S.-F. Wang, Y.-B. Zhu, Z. Liu, Y.-L. Zhou, Q. Zhang, Z.-H. Chen, H.-B. Lu, G.-Z. Yang, Chinese Phys. Lett. 20 (2003) 1356.